Biomechanical Energy Harvesting: Generating Electricity During Walking with Minimal User Effort

J. M. Donelan, *et al.*

Science **319**, 807 (2008);
DOI: 10.1126/science.1149860

study indicates that changes in resource traits influence food web diversity and complexity by interacting with foraging biology (indicated by size-dependent parasitism and sex allocation) of consumers across several trophic levels through a cascade of density- and trait-mediated effects (Fig. 2), with implications for food web stability and ecosystem functioning.

References and Notes

1. M. D. Hunter, P. W. Price, *Ecology* **73**, 724 (1992).
2. O. J. Schmitz, P. A. Hambäck, A. P. Beckerman, *Am. Nat.* **155**, 141 (2000).
3. L. Oksanen, S. D. Fretwell, J. Arruda, P. Niemalä, *Am. Nat.* **118**, 240 (1981).
4. J. M. Montoya, S. L. Pimm, R. V. Solé, *Nature* **442**, 259 (2006).
5. A. R. Ives, S. R. Carpenter, *Science* **317**, 58 (2007).
6. K. S. McCann, *Nature* **405**, 228 (2000).
7. A. R. Ives, B. J. Cardinale, *Nature* **429**, 174 (2004).
8. R. J. Williams, N. D. Martinez, *Nature* **404**, 180 (2000).
9. F. J. F. Van Veen, R. J. Morris, H. C. J. Godfray, *Annu. Rev. Entomol.* **51**, 187 (2006).
10. R. J. Morris, O. T. Lewis, H. C. J. Godfray, *Nature* **428**, 310 (2004).
11. A. P. Beckerman, O. L. Petchey, P. H. Warren, *Proc. Natl. Acad. Sci. U.S.A.* **103**, 13745 (2006).
12. M. Omacini, E. J. Chaneton, C. M. Ghersa, C. B. Muller, *Nature* **409**, 78 (2001).
13. N. Underwood, M. D. Rausher, *Ecology* **81**, 1565 (2000).
14. P. J. Ode, *Annu. Rev. Entomol.* **51**, 163 (2006).
15. J. A. Harvey, N. M. Van Dam, R. Gols, *J. Anim. Ecol.* **72**, 520 (2003).
16. C. Gómez-Campo, S. Prakash, in *Developments in Plant Genetics and Breeding*, C. Gomez-Campo, Ed. (Elsevier, Amsterdam, 1999), chap. 4.
17. H. C. J. Godfray, *Parasitoids: Behavioral and Evolutionary Ecology* (Princeton Univ. Press, Princeton, NJ, ed. 1, 1994), pp. 9–10.
18. C. B. Müller, I. C. T. Adriaanse, R. Belshaw, H. C. J. Godfray, *J. Anim. Ecol.* **68**, 346 (1999).
19. D. J. Sullivan, W. Völkl, *Annu. Rev. Entomol.* **44**, 291 (1999).
20. J. M. Tylianakis, T. Tscharntke, O. T. Lewis, *Nature* **445**, 202 (2007).
21. F. Bersier, C. Banasek-Richter, M. F. Cattin, *Ecology* **83**, 2394 (2002).
22. F. J. F. van Veen, C. B. Müller, J. K. Pell, H. C. J. Godfray, *J. Anim. Ecol.* **77**, 191 (2008).

23. The farm of Wageningen University prepared the field layout. G. Bukovinszkine Kiss and V. Taravel helped in collecting data. J. A. Harvey provided feral *Brassica* seeds. Food webs were drawn with code by H. C. J. Godfray. M.D. and T.B. were funded by the Netherlands Organisation for Scientific Research–Earth and Life Sciences Council (NWO-ALW, VICI grant 865.03.002) and F.J.F.vV. by the Natural Environment Research Council, UK. Voucher specimens were deposited at the Laboratory of Entomology (Wageningen University, reference number Buko2005.001).

Supporting Online Material

www.sciencemag.org/cgi/content/full/319/5864/804/DC1
Materials and Methods
SOM Text
Figs. S1 to S4
Table S1

25 July 2007; accepted 27 December 2007
10.1126/science.1148310

Biomechanical Energy Harvesting: Generating Electricity During Walking with Minimal User Effort

J. M. Donelan,[1]* Q. Li,[1] V. Naing,[1] J. A. Hoffer,[1] D. J. Weber,[2] A. D. Kuo[3]

We have developed a biomechanical energy harvester that generates electricity during human walking with little extra effort. Unlike conventional human-powered generators that use positive muscle work, our technology assists muscles in performing negative work, analogous to regenerative braking in hybrid cars, where energy normally dissipated during braking drives a generator instead. The energy harvester mounts at the knee and selectively engages power generation at the end of the swing phase, thus assisting deceleration of the joint. Test subjects walking with one device on each leg produced an average of 5 watts of electricity, which is about 10 times that of shoe-mounted devices. The cost of harvesting—the additional metabolic power required to produce 1 watt of electricity—is less than one-eighth of that for conventional human power generation. Producing substantial electricity with little extra effort makes this method well-suited for charging powered prosthetic limbs and other portable medical devices.

Humans are a rich source of energy. An average-sized person stores as much energy in fat as a 1000-kg battery (*1*, *2*). People use muscle to convert this stored chemical energy into positive mechanical work with peak efficiencies of about 25% (*3*). This work can be performed at a high rate, with 100 W easily sustainable (*1*). Many devices take advantage of human power capacity to produce electricity, including hand-crank generators as well as wind-up flashlights, radios, and mobile phone chargers (*4*). A limitation of these conventional methods is that users must focus their attention on power generation at the expense of other activities, typically resulting in short bouts of generation. For electrical power generation over longer durations, it would be desirable to harvest energy from everyday activities such as walking.

It is a challenge, however, to produce substantial electricity from walking. Most energy-harvesting research has focused on generating electricity from the compression of the shoe sole, with the best devices generating 0.8 W (*4*). A noteworthy departure is a spring-loaded backpack (*5*) that harnesses the vertical oscillations of a 38-kg load to generate as much as 7.4 W of electricity during fast walking. This device has a markedly low "cost of harvesting" (COH), a dimensionless quantity defined as the additional metabolic power in watts required to generate 1 W of electrical power

$$\mathrm{COH} = \frac{\Delta\ \text{metabolic power}}{\Delta\ \text{electrical power}} \qquad (1)$$

where Δ refers to the difference between walking while harvesting energy and walking while carrying the device but without harvesting energy. The COH for conventional power generation is simply related to the efficiency with which (i) the device converts mechanical work to electricity and (ii) muscles convert chemical energy into positive work

$$\mathrm{COH}\ \underset{\text{generation}}{\text{for conventional}} = \frac{\Delta\ \text{metabolic power}}{\Delta\ \text{electrical power}}$$

$$= \frac{1}{\text{device eff} \times \text{muscle eff}} \qquad (2)$$

The backpack's device efficiency is about 31% (*5*), and muscle's peak efficiency is about 25% (*3*), yielding an expected COH of 12.9. But the backpack's actual COH of 4.8 ± 3.0 (mean ± SD) is less than 40% of the expected amount. Its economy appears to arise from reducing the energy expenditure of walking with loads (*6*, *7*). No device has yet approached the power generation of the backpack without the need to carry a heavy load.

We propose that a key feature of how humans walk may provide another means of economical energy harvesting. Muscles cyclically perform positive and negative mechanical work within each stride (Fig. 1A) (*8*). Mechanical work is required to redirect the body's center of mass between steps (*9*, *10*) and simply to move the legs back and forth (*11*, *12*). Even though the average mechanical work performed on the body over an entire stride is zero, walking exacts a metabolic cost because both

[1]School of Kinesiology, Simon Fraser University (SFU), Burnaby, BC V5A 1S6, Canada. [2]Department of Physical Medicine and Rehabilitation, University of Pittsburgh, Pittsburgh, PA 15213, USA. [3]Departments of Mechanical Engineering and Biomedical Engineering, University of Michigan, Ann Arbor, MI 48109, USA.

*To whom correspondence should be addressed. E-mail: mdonelan@sfu.ca

positive and negative muscle work require metabolic energy (*3*). Coupling a generator to leg motion would generate electricity throughout each cycle, increasing the load on the muscles during acceleration but assisting them during deceleration (Fig. 1B). Although generating electricity during the acceleration phase would exact a substantial metabolic cost, doing so during the deceleration phase would not, resulting in a lower COH than for conventional generation. An even lower COH could be achieved by selectively engaging the generator only during deceleration (Fig. 1C), similar to how regenerative braking generates power while decelerating a hybrid car (*13*). Here, "generative braking" produces electricity without requiring additional positive muscle power (*14*). If implemented effectively, metabolic cost could be about the same as that for normal walking, so energy would be harvested with no extra user effort (*15*).

We developed a wearable, knee-mounted prototype energy harvester to test the generative-braking concept (Fig. 2). Although other joints might suffice, we focused on the knee because it performs mostly negative work during walking (*16*). The harvester comprises an orthopedic knee brace configured so that knee motion drives a gear train through a one-way clutch, transmitting only knee extension motion at speeds suitable for a dc brushless motor that serves as the generator (*17*). For convenient testing, generated electrical power is then dissipated with a load resistor rather than being used to charge a battery. The device efficiency, defined as the ratio of the electrical power output to the mechanical power input, was empirically estimated to be no greater than 63%, yielding an estimated COH for conventional generation of 6.4 (Eq. 2). A potentiometer senses knee angle, which is fed back to a computer controlling a relay switch in series with the load resistor, allowing the electrical load to be selectively disconnected in real time. For generative braking, we programmed the harvester to engage only during the end of the swing phase (Fig. 3), producing electrical power while simultaneously assisting the knee flexor muscles in decelerating the knee. We compared this mode against a continuous-generation mode that harvests energy whenever the knee is extending (*18*). We could also manually disengage the clutch and completely decouple the gear train and generator from knee motion. This disengaged mode served as a control condition to estimate the metabolic cost of carrying the harvester mass, independent of the cost of generating electricity.

Energy-harvesting performance was tested on six male subjects who wore a device on each leg while walking on a treadmill at 1.5 m s^{-1}. We estimated metabolic cost using a standard respirometry system and measured the electrical power output of the generator (Fig. 3C). In the continuous-generation mode (Fig. 4A), subjects generated 7.0 ± 0.7 W of electricity with an insignificant 18 ± 24 W (P = 0.07) increase in metabolic cost over that of the control condition (*19*). In the generative-braking mode (Fig. 4B), subjects generated 4.8 ± 0.8 W of electricity with an insignificant 5 ± 21 W increase in metabolic cost as compared with that of the control condition (P = 0.6). For context, this electricity is sufficient to power 10 typical cell phones simultaneously (*5*). The results dem-

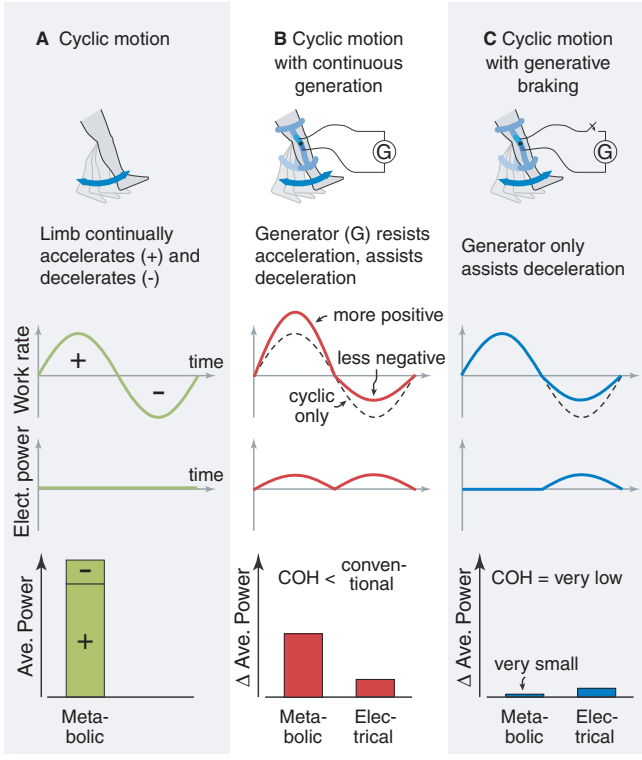

Fig. 1. Theoretical advantages of generative braking during cyclic motion, comparing the back-and-forth motion of the knee joint without power generation (**A**) against a generator operating continuously (**B**) and against a generator operating only during braking (**C**). Each column of plots shows the rate of work performed by muscles (work rate) and the electricity (elect. power) generated over time, as well as the average metabolic power expended by the human and the resulting average electrical power (ave. power bar graphs). In (B) and (C), work rate is compared against that for (A), denoted by dashed lines, and average power is shown as the difference (Δ ave. power) with respect to (A). COH is defined as the ratio of the electrical to metabolic Δ ave. powers.

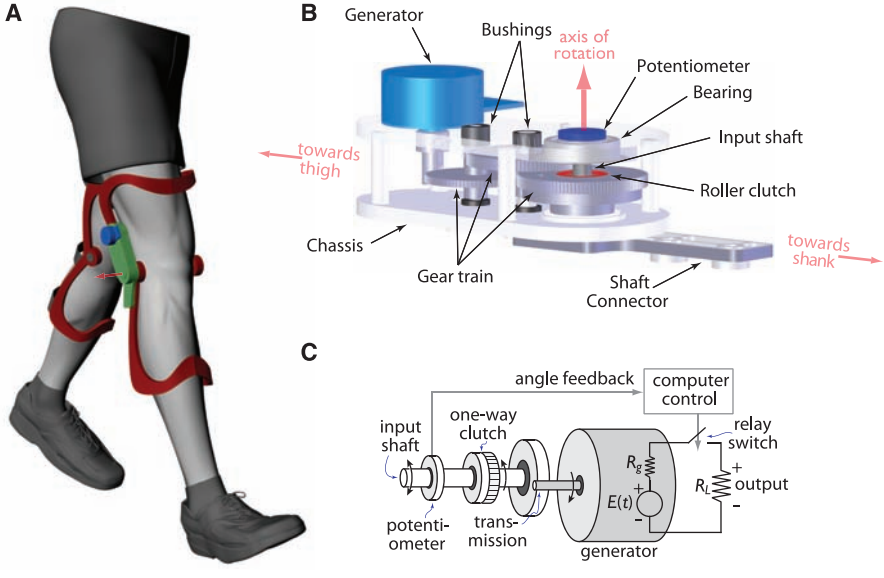

Fig. 2. Biomechanical energy harvester. (**A**) The device has an aluminum chassis (green) and generator (blue) mounted on a customized orthopedic knee brace (red), totaling 1.6-kg mass, with one worn on each leg. (**B**) The chassis contains a gear train that converts low velocity and high torque at the knee into high velocity and low torque for the generator, with a one-way roller clutch that allows for selective engagement of the gear train during knee extension only and no engagement during knee flexion. (**C**) The schematic diagram shows how a computer-controlled feedback system determines when to generate power using knee-angle feedback, measured with a potentiometer mounted on the input shaft. Generated power is dissipated in resistors. R_g, generator internal resistance; R_L, output load resistance; $E(t)$, generated voltage.

onstrate that substantial electricity could be generated with minimal increase in user effort.

The corresponding COH values highlight the advantage of generative braking (Fig. 4). Average COH in generative braking was only 0.7 ± 4.4; less than 1 W of metabolic power was required to generate 1 W of electricity. This is significantly less than the COH of 6.4 expected for conventional generation ($P = 0.01$). The COH in continuous generation, 2.3 ± 3.0, was also significantly lower than that for conventional generation ($P = 0.01$), indicating that the former mode also generated some of its electricity from the deceleration of the knee. The difference between the two modes, 2.2 ± 0.7 W of electricity, came at a difference in metabolic cost of 13 ± 12 W ($P = 0.05$). A COH taken from the average ratio of these differences yields 5.7 ± 6.2, which is nearly the same as that expected of conventional generation ($P = 0.4$). This indicates that continuous generation of power at the knee during walking produces electricity partially by conventional generation with a high COH and partially by generative braking with a very low COH. But generative braking, with less than one-eighth the COH of conventional generation, benefits almost entirely from the deceleration of the knee.

This preliminary demonstration could be improved substantially. We constructed the prototype for convenient experimentation, leading to a control condition about 20% more metabolically costly than normal walking: The disengaged-clutch mode required an average metabolic power of 366 ± 63 W as compared with 307 ± 64 W for walking without wearing the devices. The increase in cost is due mainly to the additional mass and its location, because the lower a given mass is placed, the more expensive it is to carry (*20*, *21*). Although the current increase in metabolic cost is unacceptably high for most practical implementations, revisions to improve the fit, weight, and efficiency of the device can not only reduce the cost but also increase the generated electricity. A generator designed specifically for this application could have lower internal losses and require a smaller, lighter gear train. Commercially available gear trains can have much lower friction and higher efficiency, in more compact and lightweight forms. Relocating the device components higher would decrease the metabolic cost of carrying that mass. A more refined device would also benefit from a more form-fitting knee brace made out of a more lightweight material such as carbon fiber.

Several potential applications are especially suited for generative braking. These include lighting and communications needs for the quarter of the world's population who currently live without electricity supply (*22*). Innovative prosthetic knees and ankles use motors to assist walking, but battery technology limits their power and working time (*23*–*25*). Energy harvesters worn on human joints may prove useful for powering the robotic artificial joints. In implantable devices, such as neurostimulators and drug pumps, battery power limits device sophistication, and battery replacement requires surgery (*26*). A future energy harvester might be implanted alongside such a device, perhaps in parallel with a muscle, and use generative braking to provide substantial power indefinitely. Generative braking might then find practical applications in forms very different from that demonstrated here.

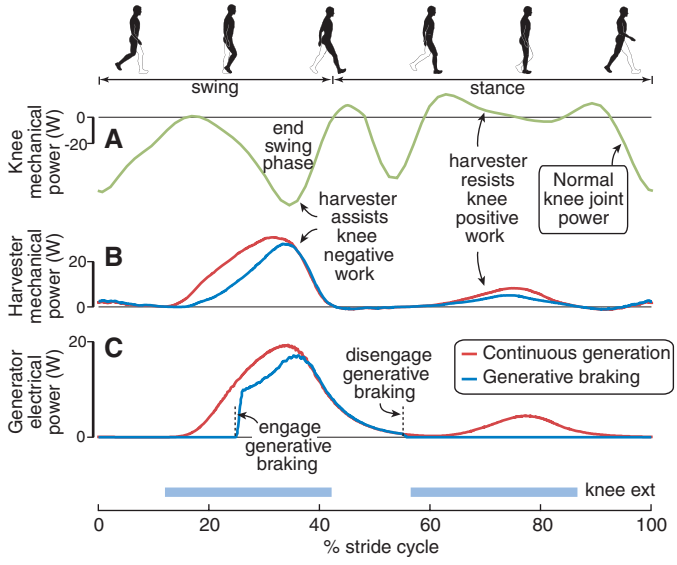

Fig. 3. Timing of power generation during walking. Time within a stride cycle, beginning with the swing phase, is shown at the bottom. The shaded bars indicate when the knee is extending and the energy harvester's clutch is engaged. (**A**) The pattern of knee mechanical power during normal walking illustrates that the knee typically generates a large amount of negative power at the end of the swing phase (*16*). (**B**) Mechanical power performed on the harvester over time, shown for continuous generation (red line) and generative braking (blue line). (**C**) Generated electrical power over time, also for both types of generation.

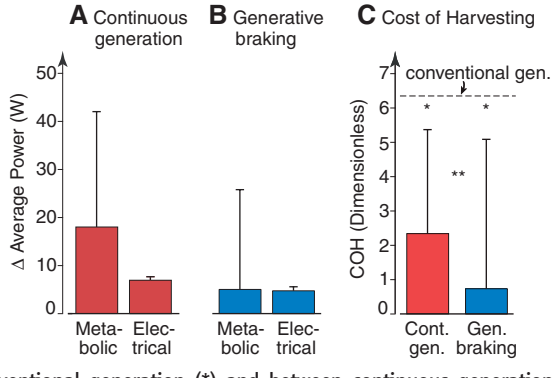

Fig. 4. Average metabolic cost and generated electricity for continuous generation (**A**) and generative braking (**B**), with change in metabolic cost (Δ average power) shown relative to the control condition. (**C**) COH (see Fig. 1) for continuous generation and generative braking as compared against that for conventional generation (dashed line). In both modes, a fraction of the harvested energy is generated from the deceleration of the knee rather than directly from muscle action. Error bars in (A) to (C) indicate SD. Asterisks indicate significant differences with conventional generation (*) and between continuous generation and generative braking (**) ($P < 0.05$ for all comparisons).

References and Notes

1. G. A. Brooks, T. D. Fahey, K. M. Baldwin, *Exercise Physiology: Human Bioenergetics and Its Applications* (McGraw-Hill, Boston, ed. 4, 2005).
2. T. Starner, *IBM Syst. J.* **35**, 618 (1996).
3. R. Margaria, *Int. Z. Angew. Physiol.* **25**, 339 (1968).
4. J. A. Paradiso, T. Starner, *IEEE Pervasive Comput.* **4**, 18 (2005).
5. L. C. Rome, L. Flynn, E. M. Goldman, T. D. Yoo, *Science* **309**, 1725 (2005).
6. A. D. Kuo, *Science* **309**, 1686 (2005).
7. L. C. Rome, L. Flynn, T. D. Yoo, *Nature* **444**, 1023 (2006).
8. H. Elftman, *Am. J. Physiol.* **125**, 339 (1939).
9. A. D. Kuo, J. M. Donelan, A. Ruina, *Exerc. Sport Sci. Rev.* **33**, 88 (2005).
10. R. Margaria, *Biomechanics and Energetics of Muscular Exercise* (Clarendon, Oxford, 1976).
11. J. Doke, J. M. Donelan, A. D. Kuo, *J. Exp. Biol.* **208**, 439 (2005).
12. R. L. Marsh, D. J. Ellerby, J. A. Carr, H. T. Henry, C. I. Buchanan, *Science* **303**, 80 (2004).
13. N. Demirdoven, J. Deutch, *Science* **305**, 974 (2004).
14. We have chosen terminology that distinguishes generative braking from regenerative braking because the electricity produced in regenerative braking is reused to power the motion of the hybrid automobile. In generative braking, the electricity is not reused to power walking.
15. Knee-joint power has contributions from forces generated by muscle fibers, tendons, connective tissue, and other passive soft tissues. The actual change in metabolic cost with generative braking depends on the relative contribution of muscle fibers to decelerating the knee joint. If muscle fibers are generating the negative power, a reduction in metabolic cost is expected. This is also true if muscle fibers are active but isometric. If the deceleration is due entirely to passive forces from elastic and plastic deformations of soft tissues, no change in metabolic cost is expected. What actually occurs at the knee during the end of the swing phase is unclear, precluding a quantitative prediction of the change in metabolic cost.
16. D. A. Winter, *Biomechanics and Motor Control of Human Movement* (Wiley, New York, ed. 2, 1990).
17. Additional methodological details, results, and videos are available as supporting material on *Science* Online.
18. The one-way clutch prevents the device from generating electricity from flexion. Nevertheless, we refer to this mode as continuous generation because, unlike the generative-braking mode, electricity is continually generated from extension regardless of whether the motion is accelerating or decelerating.

19. We used *t* tests to determine whether there was a statistical difference between conditions with an alpha level of 0.05. All electrical power comparisons were statistically significant.
20. R. C. Browning, J. R. Modica, R. Kram, A. Goswami, *Med. Sci. Sports Exerc.* **39**, 515 (2007).
21. R. G. Soule, R. F. Goldman, *J. Appl. Physiol.* **27**, 687 (1969).
22. International Energy Agency, *World Energy Outlook* (IEA Books, Paris, 2006).
23. D. Berry, *Phys. Med. Rehabil. Clin. N. Am.* **17**, 91 (2006).
24. J. L. Johansson, D. M. Sherrill, P. O. Riley, P. Bonato, H. Herr, *Am. J. Phys. Med. Rehabil.* **84**, 563 (2005).
25. R. Seymour *et al.*, *Prosthet. Orthot. Int.* **31**, 51 (2007).
26. O. Soykan, in *Business Briefing: Medical Device Manufacturing and Technology*, E. Cooper, Ed. (World Markets Research Centre, London, 2002), pp. 76–80.
27. Supported by a Natural Sciences and Engineering Research Council (NSERC) grant I2IPJ/326586-05 to J.M.D. and J.A.H., a Michael Smith Foundation for Health Research (MSFHR) Scholar Award to J.M.D., a Canadian Institutes of Health Research New Investigator Award to J.M.D., a MSFHR Postdoctoral Trainee Award to Q.L, and an NSERC Undergraduate Student Researcher Award to V.N. We thank Ossur for providing the knee braces, as well as S. H. Collins, R. Kram, A. Ruina, and the SFU Locomotion Lab for their helpful comments and suggestions. J.M.D. is chief science officer and board member of Bionic Power, Incorporated. J.M.D., Q.L., J.A.H., D.J.W., and A.D.K. have equity interest in Bionic Power, Incorporated, which performs research and development on the energy-harvesting technology reported in this paper.

Supporting Online Material

www.sciencemag.org/cgi/content/full/319/5864/807/DC1
Materials and Methods
Figs. S1 to S3
Table S1
References
Movies S1 to S4

29 August 2007; accepted 3 January 2008
10.1126/science.1149860

Three-Dimensional Super-Resolution Imaging by Stochastic Optical Reconstruction Microscopy

Bo Huang,[1,2] Wenqin Wang,[3] Mark Bates,[4] Xiaowei Zhuang[1,2,3]*

Recent advances in far-field fluorescence microscopy have led to substantial improvements in image resolution, achieving a near-molecular resolution of 20 to 30 nanometers in the two lateral dimensions. Three-dimensional (3D) nanoscale-resolution imaging, however, remains a challenge. We demonstrated 3D stochastic optical reconstruction microscopy (STORM) by using optical astigmatism to determine both axial and lateral positions of individual fluorophores with nanometer accuracy. Iterative, stochastic activation of photoswitchable probes enables high-precision 3D localization of each probe, and thus the construction of a 3D image, without scanning the sample. Using this approach, we achieved an image resolution of 20 to 30 nanometers in the lateral dimensions and 50 to 60 nanometers in the axial dimension. This development allowed us to resolve the 3D morphology of nanoscopic cellular structures.

Far-field optical microscopy offers three-dimensional (3D) imaging of biological specimens with minimal perturbation and biomolecular specificity when combined with fluorescent labeling. These advantages make fluorescence microscopy one of the most widely used imaging methods in biology. The diffraction barrier, however, limits the imaging resolution of conventional light microscopy to 200 to 300 nm in the lateral dimensions, leaving many intracellular organelles and molecular structures unresolvable. Recently, the diffraction limit has been surpassed and lateral imaging resolutions of 20 to 50 nm have been achieved by several "super-resolution" far-field microscopy techniques, including stimulated emission depletion (STED) and its related RESOLFT (reversible saturable optically linear fluorescent transitions) microscopy (*1*, *2*); saturated structured illumination microscopy (SSIM) (*3*); stochastic optical reconstruction microscopy (STORM) (*4*, *5*); photoactivated localization microscopy (PALM) (*6*, *7*); and other methods using similar principles (*8*–*10*).

Although these techniques have improved 2D image resolution, most organelles and cellular structures cannot be resolved without high-resolution imaging in all three dimensions. Three-dimensional fluorescence imaging is most commonly performed using confocal or multiphoton microscopy, the axial resolution of which is typically in the range of 500 to 800 nm (*11*, *12*). The axial imaging resolution can be improved to roughly 100 nm by 4Pi and I^{5}M microscopy (*13*–*15*). Furthermore, an axial resolution as high as 30 to 50 nm has been obtained with STED along the axial direction using the 4Pi illumination geometry, but the same imaging scheme does not provide super resolution in the lateral dimensions (*1*).

Here, we demonstrate 3D STORM imaging with a spatial resolution that is 10 times better than the diffraction limit in all three dimensions without invoking sample or optical-beam scanning. STORM and PALM rely on single-molecule detection (*16*) and exploit the photoswitchable nature of certain fluorophores to temporally separate the otherwise spatially overlapping images of numerous molecules, thereby allowing the high-precision localization of individual molecules (*4*–*7*, *9*). Limited only by the number of photons detected (*17*), localization accuracies as high as 1 nm can be achieved in the lateral dimensions for a single fluorescent dye at ambient conditions (*18*). Not only can the lateral position of a particle be determined from the centroid of its image (*19*, *20*), the shape of the image also contains information about the particle's axial (*z*) position. Nanoscale localization accuracy has been achieved in the *z* dimension by introducing defocusing (*21*–*24*) or astigmatism (*25*, *26*) into the image, without substantially compromising the lateral positioning capability.

In this work, we used the astigmatism imaging method to achieve 3D STORM imaging. To this end, a weak cylindrical lens was introduced into the imaging path to create two slightly different focal planes for the *x* and *y* directions (Fig. 1A) (*25*, *26*). As a result, the ellipticity and orientation of a fluorophore's image varied as its position changed in *z* (Fig. 1A): When the fluorophore was in the average focal plane [approximately halfway between the *x* and *y* focal planes where the point spread function (PSF) has equal widths in the *x* and *y* directions], the image appeared round; when the fluorophore was above the average focal plane, its image was more focused in the *y* direction than in the *x* direction and thus appeared ellipsoidal with its long axis along *x*; conversely, when the fluorophore was below the average focal plane, the image appeared ellipsoidal with its long axis along *y*. By fitting the image with a 2D elliptical Gaussian function, we obtained the *x* and *y* coordinates of the peak position as well as the peak widths w_x and w_y, which in turn allowed the *z* coordinate of the fluorophore to be unambiguously determined.

To experimentally generate a calibration curve of w_x and w_y as a function of *z*, we immobilized Alexa 647–labeled streptavidin molecules or quantum dots on a glass surface and imaged individual molecules to determine the w_x and w_y values as the sample was scanned in *z* (Fig. 1B). In 3D STORM analysis, the *z* coordinate of each photoactivated fluorophore was then determined by comparing the measured w_x and w_y values of its image with the calibration curves. In addition, for samples immersed in aqueous solution on a glass substrate, all *z* localizations were rescaled by a factor

[1]Howard Hughes Medical Institute, Harvard University, Cambridge, MA 02138, USA. [2]Department of Chemistry and Chemical Biology, Harvard University, Cambridge, MA 02138, USA. [3]Department of Physics, Harvard University, Cambridge, MA 02138, USA. [4]School of Engineering and Applied Sciences, Harvard University, Cambridge, MA 02138, USA.

*To whom correspondence should be addressed. E-mail: zhuang@chemistry.harvard.edu